Anisotropic Internucleosome Interactions and Geometrical Constraints in the Organization of Chromatin

Giorgio Cinacchi

Università di Pisa, Dipartimento di Chimica e Chimica Industriale, Via Risorgimento 35, 56126 Pisa, Italy

Giovanni La Penna

Consiglio Nazionale delle Ricerche, Istituto per la Chimica dei Composti Organo-Metallici, Via Madonna del Piano 10, 50019 Sesto Fiorentino (FI), Italy

Angelo Perico*

Consiglio Nazionale delle Ricerche, Istituto per lo Studio delle Macromolecole, Via De Marini 6, 16149 Genova, Italy

Received June 18, 2007; Revised Manuscript Received September 12, 2007

ABSTRACT: Chromatin structure at the high-density characteristic of the silent phase is strongly influenced by the packing of nucleosome core particles (NCPs), the anisotropic attractive interactions between two of them and constraints, such as the DNA length and bending, imposed to the wrapped and linker DNA segments. In this work, coarse-grained models of chromatin are studied. For a pair of NCPs, a simple single-site anisotropic potential energy function is designed on the basis of the experimental data reported for the ordered phases of NCPs. This potential energy function is employed in random-walks of chromatin models where the NCP DNA wrapping is modulated in length, while the linker segments are modulated in both length and curvature. For chromatin in the absence of linker histones, these models support a two-start helical organization characterized by poorly bent linkers and by a moderate reduction of wrapped DNA in the NCP.

1. Introduction

The investigation of the supramolecular structure and dynamics of chromatin is of extreme importance to understand gene regulation and cell development. The genetic information in eukaryotic chromosomes is organized in chromatin, a chainlike supramolecular assembly formed by a long filament of DNA wrapped around globular octameric aggregates of eight histone proteins.[1−3] The repeat unit of this chain includes a nucleosome core particle (i.e., the complex of a protein histone octamer with DNA wrapped around it, NCP hereafter) and a DNA linker, which connects two NCPs. Other histone proteins in the linker region are present in the natural chromatin and absent in several model systems studied in vitro. The NCP structure is well-known from high-resolution X-ray crystallography and can be summarized as a disk of radius of 5.5 nm and a height of 6 nm around which a 138−147 bp DNA is wrapped in 1.68−1.75 turns.[4,5] The linker DNA may have different lengths around an average of 50 bp.[6,7] At low ionic strength chromatin, is found as a 10 nm filament which condenses, with increasing ionic strength, in a 30 nm filament.[1] Nevertheless, the detailed structure of these chromatin states is only partially known because the conformational disorder does not allow to obtain a defined X-ray structure. Chromatin structural plasticity has probably a relevant biological meaning.

Two classes of organizations have been proposed for the compact state of chromatin (see refs 3 and 8 for recent review articles). In the first organization, the one-start solenoidal helix model, the nearest neighbors NCPs are also next in the sequence and arranged in a face-to-face configuration.[9] In the second organization, the two-start helix model, the NCPs are assembled in two coiled helices: the two nearest neighbors NCPs belong to the same helix, while two NCPs next in the sequence belong to the two different helices.[7,10−12] This model corresponds to one of the possible constructions known as crossed-linker or zigzag model.

Recent crystallographic results for the tetranucleosome molecule in the absence of linker histones,[13] provide strong evidence for the two-start helix organization: the structure of the tetranucleosome is consistent with an idealized model where two left-handed twisted ribbons follow a straight fiber axis. Yet, the debate on the relevance of linker histones in the chromatin packing is very active and the one-start solenoidal helix is consistent with many experimental findings.[8,14] In this respect, chromatin computational and theoretical modeling can be of great help.

Theoretical models of DNA supercoiling[15,16] and of chromatin structure [7,17−20] have been proposed. Among these latter models, those based on two angles provided the simplest constructions of chromatin structures consistent with the fiber density and thickness in the condensed state.[17] Further computational models[21,22] allowed the inclusion of details that can be relevant in discriminating between the several possible dense structures satisfying the constraints of the 30 nm fiber.

In ref 22, an anisotropic single-site pairwise interaction potential, originated in the field of liquid crystals, was used for the first time for modeling the effective interactions between NCPs. Constant temperature Monte Carlo simulations suggested a crossed-linker organization for the polynucleosome and significant deviations from the solenoidal structure. The same interaction has been used in related models,[23,24] where the anisotropic interaction has been combined with the modulation

* Author for correspondence. E-mail: perico@ge.ismac.cnr.it.

10.1021/ma071343l CCC: $37.00
Published on Web 11/22/2007

of the linker length. In one of the models, a two-start organization was shown.

Experimental studies of NCP systems (i.e., with no linker DNA) revealed a high propensity for phases characterized by extended columns arranged in a lattice.[25−27] These columns are organized in a lamellar phase at low ionic strength, while hexagonal columnar liquid-crystalline and crystalline phases are observed at higher ionic strength. The transition between the lamellar and columnar phases was also addressed theoretically.[28] Moreover, columnar nematic and isotropic phases were characterized, respectively at high ionic strengths and irrespective of the ionic strength value. In the interactions responsible of such ordered phases, the complicated charge distribution on the nucleosome core particles[21] and, presumably, the flexibility of histone N-terminal charged tails[29] play a determinant role. Nevertheless, well tuned anisotropic single-site interaction potentials may introduce in models certain properties of the ordered phases measured experimentally. These anisotropic interaction potentials can give a measure of the packing energy when other topological constraints of the wrapped and linker DNA segments are included into the model. Models where excluded volume contributions were added to geometrical constructions of chromatin structures have been reported,[19,20] but two-start helices with the geometry of the X-ray data were never identified among the constructed structures.

In this work, we discuss a new chromatin model. The model takes advantage of recent results in the evaluation of salt mediated electrostatic interactions in chromatin.[3,30−33] These results demonstrate the bendability of linker DNA and the strong screening of the charge carried by NCP and by linker DNA, implying a marginal role of direct electrostatic interactions linker−linker, NCP−NCP, and linker−NCP. In these circumstances, the forces determining the organization of chromatin in physiological conditions, reduce to anisotropic Lennard-Jones type interactions between NCPs and the excluded volume forces between different linkers. The residual soft electrostatic forces, explicitly ignored here, are taken better into account indirectly by a fine parametrization of several geometrical constraints, which give the model a relevant plasticity. The range and energy functions, contained in the anisotropic Lennard-Jones single-site interaction potential expression, are expanded in a proper set of functions. The expansion coefficients are tuned, through Monte Carlo simulations of a pure system of modeled NCPs, to qualitatively reproduce corresponding available experimental data for values of the ionic strength typical of physiological conditions. This interaction potential is then used to perform random walks, i.e., Markov chains based on the Metropolis test with random temperature, of chromatin models with a variable amounts of wrapped and linker DNA segments and with linker DNA with variable curvature. The position of the center of curvature and the extent of linker DNA bending, together with the length of the wrapped and linker DNA segments, are crucial parameters that modulate the NCP density in chromatin. Among the origin of bending of linker DNA, the electrostatic interactions with H3 and H4 histone N-terminal tails have been proposed.[29,31,33−35] These positively charged histone tails can be located relatively far from the NCP and they can affect extended linker portions as well as interact with nearby NCPs. The geometrical parameters that characterize our model add significant information to the previously applied models.[19,20,22,24] The results of this model will deal mainly in reconciling anisotropic NCP−NCP interactions, geometrical constraints of DNA (both in the NCP and linker regions) and the most recent X-ray data of the tetranucleosome.[13]

The results of several parametrizations of the chromatin model are reported and discussed in section 3. The model displays a high propensity for two-start organization of the dense fiber and no propensity for one-start organization, as concluded in section 4. In section 2, the calibration of the interaction potential function parameters and the construction of chromatin chains are described in details.

2. Methods

2.1. The Anisotropic Interaction between NCPs. NCPs have been modeled as cylindrically symmetric disks interacting via soft repulsive and attractive interactions. The explicit form of the interaction potential energy function between NCPs i and j, U_{ij}, is the following:

$$U_{ij}(\hat{\mathbf{u}}_i, \hat{\mathbf{u}}_j, \mathbf{r}_{ij}) = 4\epsilon_0\epsilon(\hat{\mathbf{u}}_i, \hat{\mathbf{u}}_j, \hat{\mathbf{r}}_{ij})\left[\left(\frac{\sigma_0}{r_{ij} - \sigma_0\sigma(\hat{\mathbf{u}}_i, \hat{\mathbf{u}}_j, \hat{\mathbf{r}}_{ij}) + \sigma_0}\right)^{12} - \left(\frac{\sigma_0}{r_{ij} - \sigma_0\sigma(\hat{\mathbf{u}}_i, \hat{\mathbf{u}}_j, \hat{\mathbf{r}}_{ij}) + \sigma_0}\right)^{6}\right] \quad (1)$$

This formula is a generalization to anisotropic particles of the Lennard-Jones potential.[36] The class of potential energy functions comprised in eq 1, initially conceived to model the interaction between pairs of generic molecules,[37] has received a particularly widespread use in the field of liquid crystals.[38,39] Besides ϵ_0 and σ_0, the two constants having the dimensions of energy and distance, respectively, and r_{ij}, the distance between the centers of the two interacting particles, quantities already present in the traditional Lennard-Jones potential, eq 1 contains two characteristic functions $\epsilon(\hat{\mathbf{u}}_i, \hat{\mathbf{u}}_j, \hat{\mathbf{r}}_{ij})$, and $\sigma(\hat{\mathbf{u}}_i, \hat{\mathbf{u}}_j, \hat{\mathbf{r}}_{ij})$, dependent on the unit vectors, $\hat{\mathbf{u}}_i$ and $\hat{\mathbf{u}}_j$, describing the orientation of particles i and j in the laboratory frame of reference, and $\hat{\mathbf{r}}_{ij}$, describing the orientation of the interparticle distance. They regulate, respectively, the depth of the energy well and the finite distance at which energy is zero with the orientation of the interacting particles and that of the interparticle distance. In the special case of spherically symmetric pair interactions, both functions take the value of unity, thus reducing eq 1 to the Lennard-Jones potential. In the general case of anisotropic particles, certain pair configurations have an interaction potential energy and contact distance different from those characteristic of others.

Frequently, the analytical expressions of ref 37 have been used for these functions. Presently, another approach has been preferred, already employed in two computer simulation studies of discotic liquid-crystalline systems.[40,41] It consists of expanding both functions in a set of rotational invariant basis functions called S-functions:[42]

$$\epsilon(\hat{\mathbf{u}}_i, \hat{\mathbf{u}}_j, \hat{\mathbf{r}}_{ij}) = \sum_{L_iL_jJ} \epsilon_{L_iL_jJ} S_{L_iL_jJ}(\hat{\mathbf{u}}_i, \hat{\mathbf{u}}_j, \hat{\mathbf{r}}_{ij}) \quad (2)$$

$$\sigma(\hat{\mathbf{u}}_i, \hat{\mathbf{u}}_j, \hat{\mathbf{r}}_{ij}) = \sum_{L_iL_jJ} \sigma_{L_iL_jJ} S_{L_iL_jJ}(\hat{\mathbf{u}}_i, \hat{\mathbf{u}}_j, \hat{\mathbf{r}}_{ij}) \quad (3)$$

The coefficients of these expansions are to be determined to reproduce the desired well-depth and contact distances.

To fix the range quantities, one can take advantage of the well-established fact that a NCP can be schematically seen as a disk of thickness equal to 5.5 nm and a thickness-to-diameter ratio, κ, $\simeq$0.5. Thus, the value of 5.5 nm can be immediately assigned to σ_0, while for the coefficients of $\sigma(\hat{\mathbf{u}}_i, \hat{\mathbf{u}}_j, \hat{\mathbf{r}}_{ij})$ the simple and effective approach of ref 41 has been employed.

Table 1. *S*-Functions Employed in the Expansion of the Well-Depth and Contact Distance Functions (See Eqs 2 and 3 in Text), Where $a_i = \hat{\mathbf{u}}_i \cdot \hat{\mathbf{r}}_{ij}$, $a_j = \hat{\mathbf{u}}_j \cdot \hat{\mathbf{r}}_{ij}$, and $b_{ij} = \hat{\mathbf{u}}_i \cdot \hat{\mathbf{u}}_j$

$\{L_i,L_j,J\}$	$S_{L_i,L_j,J}$
000	1
*cc*2	$^3/_2a_i^2 + {}^3/_2a_j^2 - 1$
220	$^3/_2b_{ij}^2 - {}^1/_2$
222	$(1/\sqrt{70})[2 - 3(a_i^2 + a_j^2 + b_{ij}^2) + 9a_ia_jb_{ij}]$
224	$(1/4\sqrt{70})[1 + 2b_{ij}^2 - 5(a_i^2 + a_j^2) - 20a_ia_jb_{ij} + 35a_i^2a_j^2]$

For moderately low anisotropies, only the first *S*-functions are enough. Their respective coefficients have been determined by evaluating the contact distance of a few, representative arrangements of two NCP discs, imposing that $\sigma(\hat{\mathbf{u}}_i, \hat{\mathbf{u}}_j, \hat{\mathbf{r}}_{ij})$ takes these values for these selected arrangements, and solving the consequent linear algebra problem.

To fix the energy quantities, one can resort to other experimental data. With regard to the determination of the coefficients entering the expansion of $\epsilon(\hat{\mathbf{u}}_i, \hat{\mathbf{u}}_j, \hat{\mathbf{r}}_{ij})$, the starting observation is the formation of hexagonal liquid-crystalline phases by aqueous solutions of NCPs with salt concentrations comparable to that found in the nuclei of the living cells.[26,27] This mesophase is preceded at lower NCP density by an isotropic phase, while at higher NCP density an hexagonal crystalline phase was observed. This sequence of phases, shown by a variety of discotic liquid-crystalline systems, can be reproduced by just resorting to idealized models which represent the discotic particles with cylindrically symmetric discs, interacting via a soft repulsive and attractive pair potential as in eq 1. To be precise, the principal ingredient responsible of mesomorphic behavior is the shape anisotropy. In fact, nematic and columnar phases were observed in systems of hard-body discs.[43] However, these fundamental simulation studies reveal that a thickness-to-diameter ratio of 0.5 is not enough to observe liquid-crystalline phases, rather that this quantity should at least be equal to $^1/_{10}$. Conversely, computer simulation studies on systems of spherelike particles with anisotropic attractive interactions were shown to be able to form nematic and columnar liquid-crystalline phases.[44] This set of simulation studies, together with the above-mentioned experimental data on the phase behavior of NCP solutions, suggest that a proper effective interactions between a pair of NCP cannot disregard the inclusion of anisotropic attractive interactions. The computer simulations of ref 44 modeled the latter with the corresponding expression of ref 37 with $\kappa' = 1/5$; i.e., the well depth of the face-to-face arrangement is 5 times larger than that of the edge-to-edge arrangement. In refs 40 and 41, the same value of κ', together with $\kappa = {}^1/_3$, $\mu = 1$, and $\nu = 2$, were put in the well depth expression of ref 37, which in turn was used to determine the coefficients of eq 2. In both refs 40, 41 the phase behavior of an ensemble of disks with thickness-to-diameter ratio equal to $^1/_3$ and interacting via eq 1, with $\epsilon(\hat{\mathbf{u}}_i, \hat{\mathbf{u}}_j, \hat{\mathbf{r}}_{ij})$ and $\sigma(\hat{\mathbf{u}}_i, \hat{\mathbf{u}}_j, \hat{\mathbf{r}}_{ij})$ given by eqs 2 and 3, was studied. A high propensity to form liquid-crystalline hexagonal columnar phase was observed. Thus, it has appeared sensible to determine the coefficients of eq 2 to match the expression of ref 37 with parameters $\mu = 1$, $\nu = 2$, and $\kappa' = 0.2$ and, because of the structure of a NCP, $\kappa = 0.5$. The exact procedure adopted is the same of that used in ref 41 and already discussed above for $\sigma(\hat{\mathbf{u}}_i, \hat{\mathbf{u}}_j, \hat{\mathbf{r}}_{ij})$. It remains to fix the value of ϵ_0. In ref 45 the average NCP−NCP interaction was estimated to be ∼2.0 kcal/mol. Thus, it has appeared sensible to assign to ϵ_0 a value equal to the Boltzmann factor at room temperature. Table 1 provides the expression of the *S*-functions employed in the expansions, while Table 2 gives the corresponding parameters.

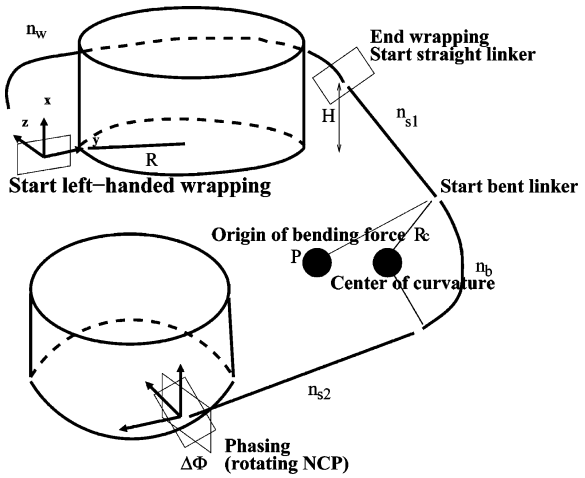

Figure 1. Schematic representation of the construction of NCP chains based on the geometry of a long curve of DNA. The parameters are: *R* and *H*, the radius and the height, respectively, of the helical segment defining the DNA wrapping around the histone octamer; n_w, number of bp wrapped; n_{s1}, number of bp on the first straight linker segment; n_b, number of bp in the bent linker segment; *P* and R_c are the origin and radius of curvature, respectively, defining the linker DNA bending; n_{s2}, the number of bp in the second part of straight linker; $\Delta\Phi$, rotation angle around the local *z* axis of the reference frame (added to the rotation imposed by B-DNA twisting).

Table 2. Parameters Entering the Expansion of the Well-Depth and Contact Distance Functions

coeff	ϵ	σ
0	0.59616195 (kcal/mol)	5.5 (nm)
000	2.06898889	1.66666667
*cc*2	3.15772555	−0.745356003
220	2.79288004	−0.152801871
222	4.04813465	−0.204190081
224	0.00021901	0.490056195

It is worth pointing out that the NCP−NCP model interaction potential energy function so developed is effective and, thus, state dependent. It is expected to be valid only for those experimental conditions on the basis of which it has been tuned, namely at physiological values of ionic strength. Liquid and liquid-crystalline phases of NCPs found at physiological conditions are not chiral, but only crystalline germs have been found with chiral properties.[26] Therefore, the interaction potential does not need to contain chiral terms for state points here investigated.

2.2. The Construction of Chromatin Chains. Chains of linked NCPs have been built according to the geometry of a long DNA segment, characterized by a wrapping length around the histone octamer (with defined wrapping geometry), a linker length and a bent linker segment in a variable position. A summary of the geometric parameters is in Figure 1, and the details about the parameters and the construction are reported below.

The chains are constructed on the basis of geometrical properties of the DNA. Once a chromatin chain is defined in terms of position and orientation of the NCPs, the anisotropic interaction potential can be used to compute the potential energy of the chain. A new configuration is proposed by random modifications of the parameters ruling the DNA geometry and the NCPs positions and orientations are derived. The potential energy of the new configuration can be used in a Metropolis test for standard Monte Carlo simulations in order to sample the canonical statistical ensemble at the given temperature, but this procedure provides low acceptance ratio for such complicated systems. Alternatively, if the Metropolis test is performed with a temperature extracted randomly within zero and a

maximum threshold, a random walk is performed, approximately sampling the density of states for the given model.[46,47] Following this second procedure, the configurations obtained through the random walk will be analyzed in this work.

The construction of the DNA pathway in the nucleosome wrapping and through the internucleosomal space, is based on successive rotations of a local frame, $\mathscr{T}$, fixed on each DNA base pair. A sketch of the construction procedure is displayed in Figure 1, where the symbols of the chain parameters are also reported. The local frame has the *z* axis as the normal of the bp plane. The *y* axis is contained in the bp plane and, at the beginning of the NCP wrapping, i.e., in $\mathscr{T}_0$, it points toward the symmetry axis of the NCP. The *x* axis is contained in the bp plane, and in $\mathscr{T}_0$ the *x* axis is parallel to the NCP cylindrical symmetry axis. Therefore, the position of the NCP center and the direction of the NCP symmetry axis are ruled by the local frame $\mathscr{T}_0$ of the first wrapping DNA bp.

The geometry of the NCP is based on three parameters: the NCP radius *R*, the NCP height *H* and the number of wrapped base pairs (n_w) provide the bending of the DNA during its wrapping. This is achieved by rotating the local DNA frame with the Euler angles (in the Goldstein convention):

$$\begin{aligned} a &= H/(n_w - 1) \\ \alpha &= -\arcsin([a^2/(R^2 + a^2)]^{1/2}) \\ b &= c/(2R) \\ \beta &= -2\arcsin(b) \\ \gamma &= 0 \end{aligned} \tag{4}$$

where *c* is the length of the pathway between two consecutive base pairs (local reference axis) in the DNA, i.e., $c = 0.34$ nm.[7] In order to match the size of the NCP particle $R = 4.5$ nm and $H = 5.7$ nm. The radius of NCP wrapping, *R*, is consistent with the usually assumed size for the histones aggregate (3.5 nm), added for the radius of the B-DNA cylinder (about 1 nm). The height of wrapping, *H*, is obtained by measuring the angle between the entering and exiting DNA axes for different trial values of *H*, while keeping $n_w = 147$. For a value of $H = 5.7$ nm (i.e., very close to the value of 6 nm usually adopted for the NCP height), the angle between the entering DNA and the exiting DNA is found at 90° (corresponding to 1.75 DNA turns). Therefore, a value of $H = 5.7$ nm was kept constant, together with $R = 4.5$ nm, for all values of n_w during simulations: the degree of wrapping is modulated only through the parameter n_w.

The phase of the local *y* axis of the DNA bp is related to the DNA twisting during the growth of the DNA chain. A constant gross value for the twisting angle of 36° between consecutive bps is assumed along the whole DNA chain,[7,48] being the change of twisting angle with wrapping and bending of DNA negligible for the present model. The change of phase of the local *y* axis is therefore related to the number of base pairs that encompass the NCP wrapping and the linker DNA. With no further information on the NCP mutual orientation, the equilibrium twisting of DNA determines the orientation of the NCP $i + 1$ with respect to NCP *i* in the chromatin chain. In the present model a further change of phase $\Delta\Phi$ is included: this is the additional twisting of DNA due to the possible change of orientation of NCP $i + 1$ with respect to the orientation determined by the equilibrium DNA twisting. The $\Delta\Phi$ parameter strongly affects the anisotropic interactions between neighbor NCPs.

In order to understand the effect of the many geometrical parameters used to build the chain of linked NCPs and to limit the variation of some of them, part of the available knowledge on chromatin structure can be used. The one-start solenoidal organization of chromatin can be summarized by the following definitions:

1. The number of DNA bp moieties wrapped around the histone octamer is 147, corresponding to 1.75 turns.

2. The linker is bent similarly to the wrapped DNA; i.e., the linker DNA follows a pathway with about the same curvature of the wrapped DNA.

3. The angle between NCP planes is small, and the NCP normal vectors are almost perpendicular to the fiber axis.

The two-start helix is characterized by a very different organization, which can be summarized by the following definitions:

1. The number of DNA bp moieties wrapped around the histone octamer is 138, corresponding to 1.67 turns.

2. The linker is locally bent in the middle of its pathway between two NCPs, as suggested by the DNA construction derived from the low-resolution crystal structure of the tetramer.

3. The angle between planes of NCPs linked together and belonging to the two different helices is about 90° and each NCP normal vector makes an angle slightly smaller than 90° with the fiber axis.

In both cases, the linker DNA can be bent and a model accounting for different extents of linker bending becomes useful for a complete investigation of possible chromatin structures. In this model, the bending of the DNA chain in the linker region is based on the position of a center of curvature determined in the frame of the NCP preceding the bent linker DNA. Since the DNA chain must have no edges (the tangent must be continuous), the curvature cannot be performed around an arbitrary point in the space. The center for the rotation is in a plane containing the straight linker DNA before the curvature and the vector joining the bp center at the beginning of curvature with the location of the hypothetical origin of bending force, i.e., the position *P* in Figure 1. This position mimics, for example, the center of the histone tail extruded from the NCP.

The radius of curvature, R_c, is kept constant during the random walks, while the position *P* is randomly suggested within a maximum displacement of ± 10 nm, in the three directions of space, around a given fixed point P_0 in the local frame $\mathscr{T}_0$ at the beginning of the NCP wrapping. Several choices of P_0 were evaluated. In this work the cases where P_0 is in (0, 0, −5) and in (*H*, *R*, 0) are discussed in detail. The first choice places the center of curvature in a region around the base plane of the NCP (see cubic region in Figure 2, panel I); the second choice places the center of curvature in a region around the top of each NCP (see cubic region in Figure 2, panel II). The large variation allowed for *P* once P_0 is located (i.e. the cubes in Figure 2) decreases the dependence of results from the location of P_0. The radius of curvature is chosen as 1 nm in the first case and 4.5 nm in the other case in order to impose, respectively, a large bending when the center of curvature is in the base plane of the NCP, and a curvature similar to the wrapped DNA when the center of curvature is on the NCP top plane. The first choice (case I, hereafter) mimics a bending imposed by a histone tail dangling in the internucleosomal region, while the second case (case II, hereafter) mimics a linker bending due to the collapse of histone tails onto the histone octamer core.

The volume, *V*, of the oligomer is calculated representing each of the anisotropic NCPs in each configuration with 11 identical spheres of radius of 2.75 nm. One sphere is placed in

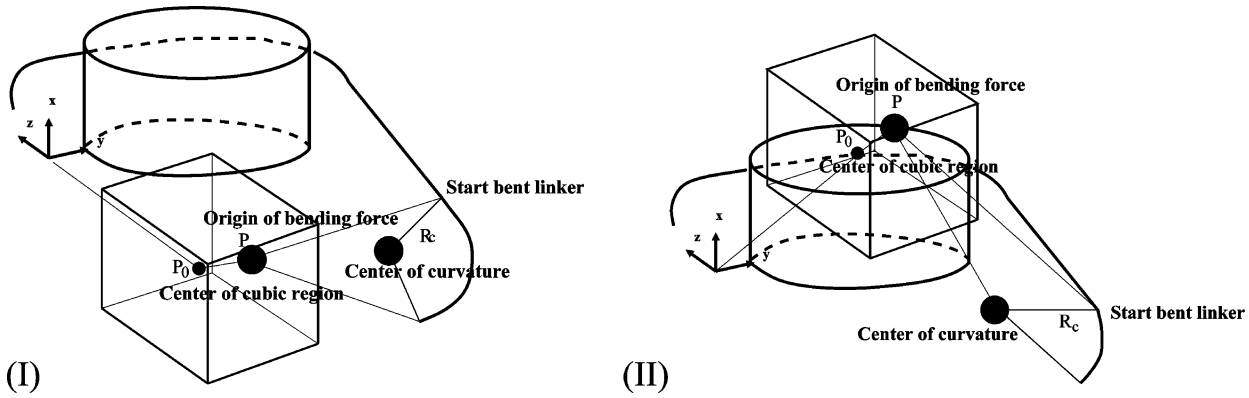

Figure 2. Schematic representation of the choice of P_0 and P in scheme of Figure 1 in case I (left) and II (right).

the center of the NCP and the other 10 spheres are placed along a circle of radius 2.75 nm. This cluster of spheres adequately represents the volume of the anisotropic NCPs that were used in the Monte Carlo simulations. The accessible surface and volume of the chain represented as a cluster of isotropic sites is measured with a spherical probe of radius 2.75 nm. The NSC code[49] was used with 300 triangles per unit sphere. As a term of comparison, the volume V_0 of N free NCPs, with N the number of NCPs in the chain, will be used in the analysis.

The interaction potential used in random walks of chromatin oligomers does not include the interactions between linker DNA segments and between the linker DNA segments and NCPs. In order to discriminate at least those structures where linker DNA segments overlap, a Lennard-Jones interaction between sites centered on each DNA bp in the linker, is used in the selection of structures for analysis. Each bp is a Lennard-Jones site with $\sigma = 1$ nm and $\epsilon = 1/10$ of the well-depth parameter for interactions between NCPs. The ϵ parameter is arbitrary because only the sign of the linker−linker potential energy will be used in the following analysis. The choice of the σ parameter one-half that expected for a B-DNA double helix slightly compensates for the lack of local DNA flexibility.

The interaction between each DNA bp and NCPs is never calculated in the present model. This interaction can be in theory calculated on the basis of the *S*-functions expansion for the interaction energy between isotropic and anisotropic sites, that can be exactly consistent with the choices of parameters chosen for NCP−NCP and linker−linker interactions. But this interaction, for linker sites attached to one NCP, would introduce spurious positive contributions which could be avoided introducing an arbitrary cut-off. Therefore, we decided to ignore this contribution at this stage.

Oligomers of 20 NCPs were constructed assuming that the geometrical parameters for NCPs and DNA linkers are the same for all the NCPs and linkers. Therefore, the chain is highly symmetrical. The random walks were constructed by randomly changing n_w, n_{s1}, n_b, and n_{s2} within given ranges. The parameter n_w was varied within 120 and 160; the total linker length, i.e., the sum $n_l = n_{s1} + n_b + n_{s2}$, was varied within 20 and 60; then n_{s1} was varied within zero and n_l, n_b was varied within zero and the difference $n_l - n_{s1}$ and n_{s2} was varied within zero and $n_l - n_{s1} - n_b$. At the end of each move, the final n_l could be, therefore, less than the initially chosen random value, but still within zero and 60. The $\Delta\Phi$ value was randomly chosen within zero and 2π.

The temperature used in the Metropolis test is randomly chosen within 0 and 10000 K. Once initial conditions for the chain parameters were given, 10 separated random walks were performed for each of the two cases analyzed in this work. Each random walk was performed for 2 000 000 collective moves and configurations were saved every 10 attempted moves. A total amount of 2 000 000 configurations were collected for each of the positions P_0 selected in the model. The acceptance ratio was about 10%. Because of the high temperatures used in the random walks and the few degrees of freedom of the homogeneous models, the dependence of results from initial conditions is negligible.

Configurations from the whole random walk were selected if they satisfy at the same time three criteria:

1. The potential energy due to anisotropic interactions measured per number of anisotropic particles (NCPs) is lower than $-30 \times \epsilon_0$, where ϵ_0 is the potential energy of the pair configuration in the energy minimum when approached side-by-side with NCP axes mutually perpendicular. Given the coefficients of the anisotropic potential, an infinite column of disklike particles corresponds to a potential energy per pair of NCPs of about $-40\ \epsilon_0$. The choice of including in the selection potential energies larger than this minimum value, allows the analysis of significantly distorted columnar configurations.

2. The volume V of the configuration, measured as explained above, is lower than $0.8 \times V_0$. This choice implies the exclusion from the analysis of configurations with low NCP density.

3. The interaction energy between linker DNA, measured via an isotropic Lennard-Jones interaction (as explained above) is lower than zero; i.e., linker DNA segments do not overlap.

3. Results

3.1. Building the Anisotropic Interactions between NCPs. Monte Carlo computer simulations in the isothermal−isobaric (*NPT*) statistical ensemble of a system of 648 disks interacting via eqs 1, 2, and 3 (see Methods) and with the parameters determined as described in the Methods section indeed gave, at room pressure, hexagonal columnar liquid-crystalline phase at values of density close to those encountered in the experiments of refs 25−27.

Order parameters, density, and enthalpy of the system were monitored as a function of temperature T. The system undergoes a phase transition from a columnar hexagonal phase to an isotropic phase at $T \sim 225$ K, as it can be estimated by monitoring the positional hexagonal bond order parameter[38] as a function of T (data not shown). For $T > 300$ K the system reaches a density in the range 268−412 mg/mL. The experimental range for the densities of all the nonhexagonal columnar phases was estimated in the range 350−400 mg/mL.[25] For $T <$ 150 K, the system, in the hexagonal columnar phase, reaches a density in the range of 530−600 mg/mL, which is only slightly

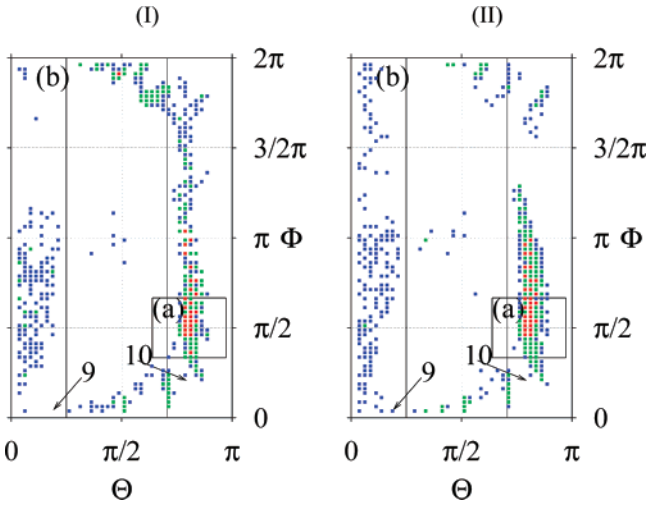

Figure 3. Distribution in Θ and Φ angles (see text) obtained from the configurations selected within the random walk for the two cases (panels I and II, respectively). Regions of maximum probability P_{max} are in red, those with $P = P_{max}/10$ are in green and $P = P_{max}/100$ are in blue. Regions of lower probability are not displayed. Regions *a* and *b* are indicated within solid-line boundaries. The region on the right of the thin vertical line indicates the region excluded for NCP as spherical sites (see text). Arrows indicate configurations 9 and 10 of Figure 20 in ref 3.

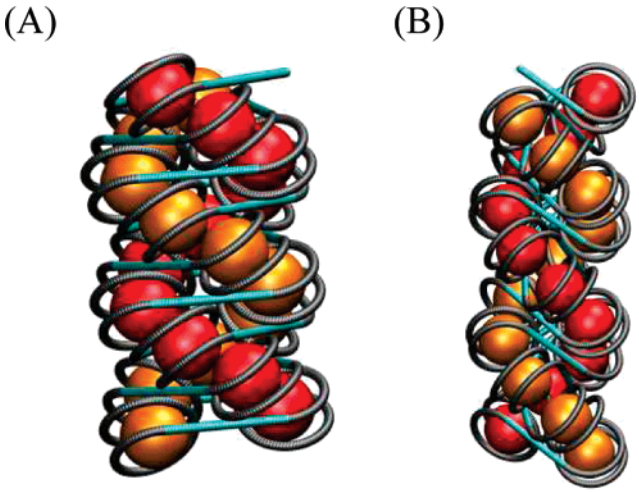

Figure 4. Configurations selected from region *a* of case I. DNA beads are of 0.5 nm radius. NCP cores (the histone octamer) are of 3.5 nm radius. To emphasize the two-start organization, NCP of even index are in red and of odd index are in orange. This and the following molecular structures were drawn with the VMD program[56] by loading extended data representations of the displayed configurations.

larger than the maximum value estimated for chromatin in vivo, i.e., about 500 mg/mL.[25] A slight decrease in NCP density can be imposed by the constraints of DNA wrapped around the histones in the actual chromatin.

We conclude that in the *NPT* Monte Carlo simulations of the single-site anisotropic model of NCPs the increase of temperature forces a phase transition that is very similar to that observed in vitro for NCPs by decreasing the osmotic pressure at the fixed monovalent salt concentration of 0.1 mM and at room temperature.[26] None of the metastable phases observed experimentally (i.e., the columnar nematic and columnar isotropic phases) are modeled, mainly because of the simplicity of the NCP interaction potential. Nevertheless, the size of the parameters used in the single-site interaction potential was sufficiently accurate to capture the major structural transition for NCPs in a concentrated solution at high ionic strength. This model NCP pair potential energy function cannot give rise to the columnar lamellar mesophase observed for real systems of NCPs at low ionic strength. For such purpose, another set of parameters, at least, if not even a different functional form, have to be developed.

3.2. Two-Angle Analysis. The first analysis is based on the structural classification proposed by Schiessel et al. on the basis of the two-angle model.[3,7,17,19] The two angles used in the analysis are: the supplementary angle to the bending angle spanned by the centers of three consecutive NCPs in the chain (Θ); the dihedral angle spanned by the centers of four consecutive NCPs in the chain (Φ). The Φ angle reported in the most recent work by Schiessel et al.,[19] is indirectly related to the linker length of Woodcock et al.,[7,17] even if in this latter case a modification in linker length acts both on the angle between NCP planes and on the NCP−NCP distance. In our model, the Θ and Φ angles are not free parameters, but they are complicated geometrical functions of the used parameters (see Figure 1). The bending and dihedral angles within NCPs in the chain allow a simple identification of some structural features on the basis of two variables.

In Figure 3, the distribution of structures within the two angles is displayed. The distribution for case I (panel I) and II (panel II) displays similar features:

1. Most of the structures are below the $\Phi = \pi$ line.

2. Both the distributions display a maximum in the region with $\Theta \sim 5\pi/6$ and $\Phi \sim \pi/2$, not far from the crossed-linker region of the two-angle model (structure "10" in Figure 20 of ref 3).

3. The region with $\Theta \sim 0$ displays a flat distribution.

The thin vertical line on the right in the figures is drawn according to the short-range excluded volume restrictions for spherical NCPs reported in refs 3 and 19: structures with $\Theta > \pi - 2a/b$ are forbidden due to sphere overlapping. In the two-angle model the parameter *a* is the radius of the NCP sphere, while in our model we choose *a* as half the side-by-side contact distance, 5.5 nm. The parameter *b* is the average of the distance between two consecutive NCPs in the chain: in the two-angle model *b* is fixed, while in our model *b* is the distance averaged over all the configurations selected from the random walk, giving the value of $b = 12$ nm.

A first feature is that the right-handed ($\Phi > \pi$) structures are less than the left-handed structures. In the model, this is the result of the left-handed DNA wrapping around the histone octamer. The left-handed wrapping is evident from X-ray data of the NCP[4] and it is the result of the chirality of the histone octamer.[50] The higher population for left-handed compared to right-handed helices found in our model is consistent with most of the electron microscopy and X-ray observation for chromatin,[11] even if there is not a clear measure of the relative abundance of the two chiral structures.[51] The chirality observed in NCP crystalline germs was in part attributed to chiral NCP−NCP interactions,[52] concluding that chiral interactions are important in the chirality of chromatin and of eukaryotic chromosomes. Within our model, where NCP−NCP interactions do not contain chiral terms, the chirality of the chromatin fiber is a result of the left-handed DNA wrapping around the histone octamer.

A second feature is that three-dimensional fibers with crossed linkers are the most abundant in our model. The structures contributing to the maximum in the distribution will be analyzed below in detail, but the proximity of the maximum to the configuration "10" in Figure 20 of ref 3 indicates the prevailing

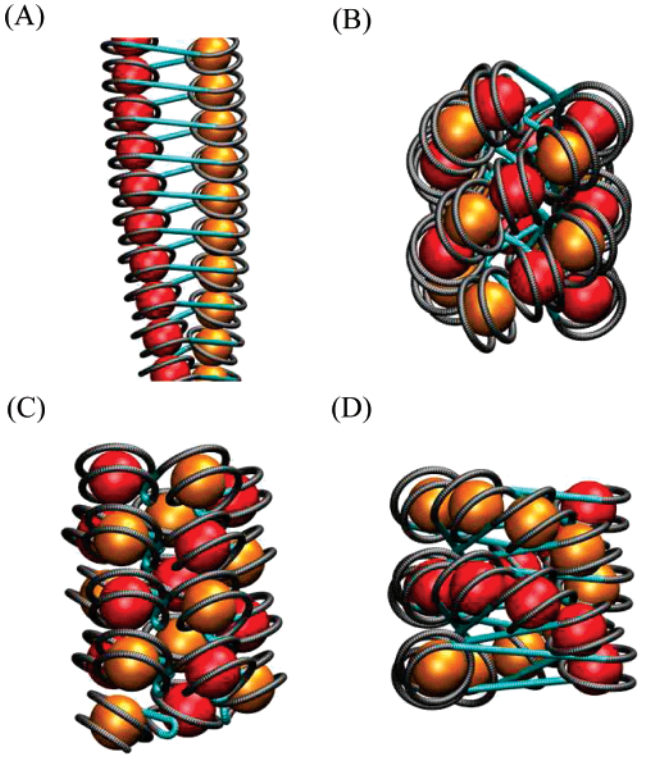

Figure 5. Configurations selected from region *c* of case I.

of this configuration. The violation of the short-range excluded volume restriction based on spherical sites with radius 5.5 nm (the thin vertical line in Figure 3) is motivated by our choice of sphere radius *a*: our choice of $a = 5.5$ nm assumes a radius of the NCP sphere that contains the anisotropic site of our model. On average, each anisotropic site behaves as an object with volume smaller than that of such sphere. The distribution displayed in the figure shows that a good effective radius *a* should be about half the chosen value: with this new choice, the thin vertical line in the figure would appear at the right of the maximum of population and the excluded region would contain only a few points of measurable population. This suggests that the face-to-face contacts dominate the excluded volume conditions.

A third feature of Figure 3, is an indication of the presence of many structures with low Θ values and arbitrary Φ values. These structures are distorted columns.

Two further important features displayed by Figure 3 are the presence of a forbidden region in between the maximum and the columns, and the lack of solenoidal structures that are expected in a region with low Θ values and Φ values restricted by the helical structure (see arrows "9" in the figure). In fact, solenoidal structures can be represented by single columns coiled in helical structures.

The difference between the distributions derived from cases I and II is significant. In case I right-handed structures are more concentrated toward crossed-linker structures, while in case II most of the right-handed structures are columnar. In case II the region of the maximum population is wider and more separated by the region of columns. This difference between cases I and II suggests possible significant effects of the nature of linker bending on the transition between left- and right-handed chromatin organizations.

3.3. Visualization of Structures. The second level of analysis is the visualization of the structures that contribute to the different regions of the distribution plotted in Figure 3. On the basis of Figure 3, three regions were identified. The first region is defined by the box $115° < \Theta < 175°$ and $60° < \Phi < 120°$ (region *a*, hereafter). The second region is defined by the limitation of $0 < \Theta < 45°$ and any Φ value (region *b*, hereafter). The third region (region *c*, hereafter) contains all the other configurations.

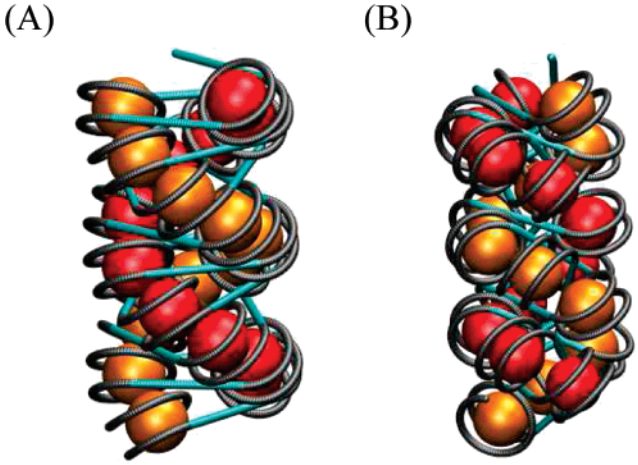

Figure 6. Configurations selected from region *a* of case II.

3.3.1. Case I. For case I, the number of configurations contained in region *a* is 55245 over the 129425 configurations selected from the original random walk, i.e., 43% of the configurations are in region *a*. In region *b* are present 6% of the configurations.

In Figure 4, two typical examples of configurations in region *a* are displayed. The organization is clearly that of a two-start helix. The distance between NCP *i* and NCP $i + 1$ is 13.0 and 11.9 nm in panels A and B, respectively. The distance between NCP *i* and $i + 2$ is 6.9 and 7.5 nm in panels A and B, respectively. The structure of panel A has two NCPs belonging to the same helix almost located at the energy minimum for the face-to-face configuration (6.2 nm). The closest distance between the two helices is slightly larger than the side-by-side distance at the minimum interaction energy (12.3 nm). In the structure of panel B the first distance is increased, but the second distance is decreased. This change is accompanied by a change in the linker orientation with respect to the fiber axis: in panel A the linker is almost perpendicular to the fiber axis, while in panel B it is more tilted toward the axis. The pitch of the double helix (i.e., the closest distance between the two helices when this distance is aligned along the fiber axis) is 12.9 and 13.6 nm in panels A and B, respectively. This means that the double helix is in both cases slightly elongated compared to both the X-ray structure of the tetranucleosome and the usual solenoidal structure. Consequently, the density of NCPs in the fiber is, for region *a* of the present model, slightly lower than that obtained for the proposed high-density structures. Nevertheless, the structures displayed in Figure 4 are very similar to the two-start organization proposed for chromatin on the basis of the X-ray data for the tetranucleosome (see Figure 3 of ref 13).

The closest face-to-face contact distance is more easily approached in columnar structures (those in region *b*). In most of the columnar structures (data not shown), the closest neighbor distance is about 6.5 nm, the linker is very short and the arrangement of DNA entry and exit points in each NCP is up−down.

It is interesting to investigate some of the structures belonging to region *c* of Figure 3. In Figure 5, four of these structures are

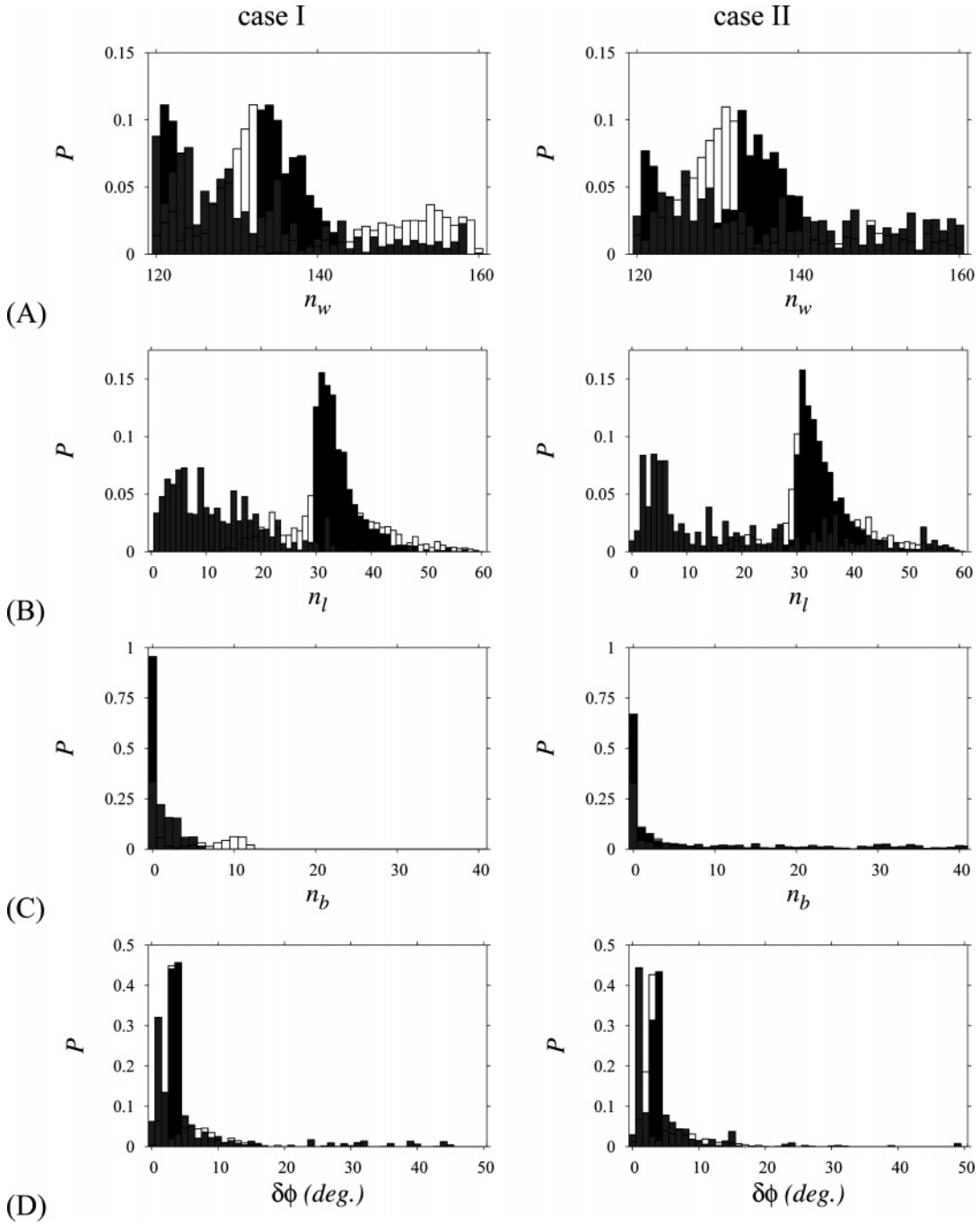

Figure 7. Distributions of n_w, n_l, n_b, and $\delta\phi$ obtained from the selection within the random walk. Contributions from region *a* (dark gray boxes), from region *b* (light gray boxes) and from region *c* (empty boxes).

displayed. Most of the structures in region *c* are of the type of that displayed in panel A: two columns arranged in a two-start organization, with weak left- or right-handed torsion. These structures are topologically well separated from the single columns, because of the significant increase in the linker length. They are more likely related to the more dense two-start organizations, displayed in Figure 4 and Figure 5D, via an increase in the coiling of both the helices (see below). Many configurations in region *c* display the organization of more than two helices, like that displayed in panel B (three helices). The few one-start solenoidal configurations (panel C) display largely bent linkers and the NCP dyad axes almost parallel to the fiber axis, two features that are not consistent with experimental data for chromatin and oligonucleosomes at high density. Note that two-start high density organizations of the fiber are also present in region *c*, mainly because of the high population of regions close to region *a* in Figure 3. In Figure 5D, one of these structures is displayed: it is very similar to those displayed in Figure 4 with the exception of a long linker (57 bp) obtained at the expense of a partial unwrapping of DNA from the NCP (123 bp are wrapped).

3.3.2. Case II. For case II, the number of configurations contained in region *a* is 77162 over 160008, that is 48% of the configurations. In region *b*, as in case I, 6% of the configurations are present. All the structural features observed for case I are very similar in case II.

In Figure 6, two structures in region *a* are displayed. The two-start helical organization of the chain is evident also in this case. The linker location is slightly less exposed in Figure 6B, where the linker DNA is more buried in the center of the double

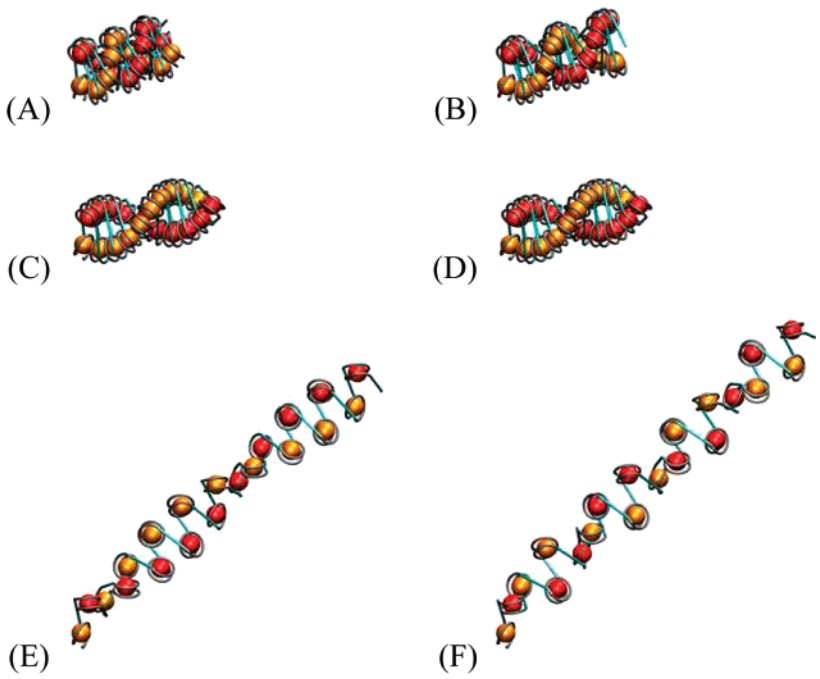

Figure 8. Configurations obtained through the unfolding of structure in Figure 4A.

helix and the orientation of the linker is slightly more parallel to the fiber axis compared to Figure 6A that is almost identical to the structure displayed in Figure 4A.

3.4. DNA Geometry. The packing of NCPs in the structures of regions *a* and *b* is related to the amount of DNA wrapped around the histone octamer and of DNA in the linker.

The contribution of different regions to the distributions of the variables in Figure 1, i.e. n_w, n_l (total number of bp in linker), and n_b, is displayed in Figure 7. Moreover, the average twisting of the linker is analyzed by mean of the variable $\delta\phi = \Delta\Phi/n_l$, that is the averaged deviation of the twisting of a DNA bp with respect to its equilibrium value in the B-DNA (36°).

In both cases I and II, the number of wrapped DNA bp is within 130 and 140 bp when configurations are in region *a* (dark gray bars in Figure 7A). The maximum of this distribution is closer to 129, found in the X-ray structure of the tetranucleosome,[13] than to 147, the usual number adopted for solenoidal one-start helices. A decrease from 147 to 129 wrapped bp has been explained with the partial unwrapping of about 9 bp from each of the entry and exit points of DNA in the NCP.[5] Moreover, in chromatin the extent of wrapped DNA is subject to significant fluctuations.[53] In the model, most of the population with $n_w >$ 140 is disfavored by the constraints provided by the selection, being the random walk distribution of n_w almost uniform within 120 and 160 bp (data not shown).

The large numbers of wrapped DNA bps when the configurations are columnar (region *b*, light gray bars in the figure) are due to the inclusion in the wrapped segments of most of the linker, that in region *b* displays $n_l < 20$ (panel B in the figure). In case II, there are many configurations with a large number of bent bps in the linker and belonging to region *b*, while in case I the bending is limited to 10 bp and all the configurations with bent linkers belong to region *c*. Finally, the twisting deviation per linker bp, $\delta\phi$, is, with the exception of a few cases, limited to 10° and for configurations of region *a* is, in both cases, even smaller (about 5°, dark gray boxes in panel D).

The main information that can be obtained by this analysis is that the structures that display a two-start organization (those in region *a*) display 130−140 bp wrapped around the histone octamer and 30−40 bp in an almost straight and only slightly twisted linker.

The structures identified as the most compact in the whole set of structures selected within the random walk, can, in theory, have knots and entangled DNA filaments.[54] In order to check if configurations like that displayed in Figure 4A (i.e., belonging to region *a*) can be unfolded without passing through configurations where DNA linkers overlap, a "smooth" pathway in the model variables was designed. The variables n_w, n_{s1}, n_b and n_{s2} were changed every MC move at maximum of ±1, Φ was changed at maximum of 3.6°, and the origin for linker bending was displaced at maximum of 0.5 nm. The linker−linker Lennard-Jones interaction was included in the potential energy and a random walk was performed as in the previous case starting from configuration displayed in Figure 4A. The random walk drives the initial configuration toward configurations with large number of ways to occur and, therefore, toward a lower NCP density and a higher NCP−NCP interaction.

In Figure 8, six configurations obtained through one of these unfolding pathways are displayed. All the configurations visited during the unfolding pathway have negative NCP−NCP and linker−linker interaction energies. The total number of bp in the linker increases of a few units, while the number of bp in the NCP wrapped region remains almost constant. The average linker twisting is in all cases lower than 4°. In conclusion, the change in all the parameters is small, while the linear NCP density in the structures decreases significantly. The two-start dense organization first is changed into a two-start organization of lower density and, eventually, the two-start organization is demolished to leave a one-start organization that resembles a stretched solenoid.

4. Conclusion

We have generated random walks, i.e., Markov chains based on the Metropolis test with random temperature, of chromatin models in physiological conditions using only anisotropic Lennard-Jones type potential between NCPs, excluded volume interactions between DNA and soft constraints derived from the structure of DNA or parametrizing the effects of residual

screened electrostatic forces. These soft constraints modulate the length of wrapped DNA around the NCP and both the length and bending of linker DNA giving to the model a relevant plasticity.

The preference of NCPs, the building blocks of the chromatin polymer, to form columns in the fluid phase is encoded in the single-site pairwise force-field used in our model. This preference is shown by studies of the liquid-crystal phases formed by NCPs, where discotic columnar phases were well characterized and a columnar nematic phase was also identified.

When used in Monte Carlo simulations, an ensemble of these mesogenic model NCPs captured the energy and density change going from the hexagonal columnar phase to the isotropic phase of real dispersions of NCPs.

The same interaction potential was then applied to chains composed by NCPs. The NCPs were constrained in their mutual distances and orientation by a single DNA molecule. The DNA is built as the pathway of a base-pair according to the DNA geometry when the DNA is wrapping around a cylinder (the NCP), or it is taken in a standard B-DNA (straight linker) or it is wrapping around a sphere (linker bending). The range for the length of the differently bent segments has been chosen within usually observed values. The anisotropic interactions between NCPs are, therefore, limited, and the columnar structures, still favored by anisotropic interactions, follow the wrapped and linker DNA constraints.

By far, the most abundant configurations of high density and low energy display the organization of two-start helix proposed on the basis of X-ray crystallography, even though the computed fiber pitch and thickness, as well as the NCP linear density, are more consistent with a slightly more elongated fiber compared to that displayed in the construction of Schalch et al. (Figure 3 of ref 13). The few one−start solenoidal structures found in the random walks display linkers with unusual bending and, in order to maximize the interactions between NCPs, the NCPs are oriented with the normal vectors of the NCP planes parallel to the fiber axis.

In addition, a few multicolumnar structures are represented in the set of high-density and low-energy configurations. The minimum energy configurations are rather independent from the location of the center of curvature in the linker region. Most of the structures have straight and poorly bent linkers.

The search for possible structures of high-density chromatin is still challenging (see ref 8 for the most recent review on this debate) and reproducible models greatly help in this investigation. The one-start organization (the solenoidal model) that emerged as a possible structure is consistent with many data about the linear NCP density, the size of the fiber, the mutual distances within NCPs, the mutual orientation of NCPs and their orientation with respect to the fiber axis. The one-start organization is still accounting for the high density of the silent phase of chromatin, and recent experiments, in the presence of one linker histone, are claimed to be consistent only with the one-start organization.[55] Even if a solenoidal organization emerged as one of the possible solutions of supercoiled DNA elastic rod model,[15,16] one of the major complication of the one−start organization was the observation that in order to adapt a straight or even moderately bent linker in the internucleosome space, the DNA should follow a complicated pathway. Recent experiments on chromatin samples, specially designed for increasing regularity and lacking of linker histones, and in particular the X-ray data at 9 Å resolution for the tetranucleosome, strongly modified the view of the DNA pathway in chromatin and of the NCPs organization. The two-start organization emerged from the analysis of these data.

The model here reported shows that for a homogeneous (and therefore regular) model of a polynucleosome a one-start helical organization is less likely than a two-start helical organization. Even if experimental evidence supporting the two-start helical model for chromatin is increasing, the one-start solenoidal model appears less intricate than the two-start helices, simpler in its construction and swelling, and more manageable in biological processes. A solenoidal structure can be viewed as a single column of facing disks coiled in a single helix. The pairwise potential used in our model favors face-to-face interactions between NCP disks, but the resulting columns can be coiled up to have a too large minimum helical pitch, like that displayed in Figure 4. The limiting value for the helical pitch is more compatible with a two-start organization, because in this latter case the helical pitch of each of the two helices is larger than in the one-start helix. Almost straight linkers can easily adapt to this organization. A higher linear NCP density in the fiber can be reached by small local adjustments of the linker segments arising for the presence of linker histones and/or for interactions of linker DNA with NCP histone tails.

The similarity of the most representative structures obtained with our model with the X-ray structure derived from the analysis of tetranucleosome data (compare Figure 4a with Figure 3b of ref 13) is the major result of this work. The evidence for two-start organization of chromatin emerged in previous models.[19,22,24] In the Monte Carlo simulations,[22] because of the irregularity of the chain, the crossing of linker segments was shown, but the two-start organization was not clearly evidenced. In the regular geometrical constructions of ref 24, the linker segments appeared as highly entangled, and this issue was not addressed. In this work we definitely address these issues: the crossed-linker structures are clearly two-start helices with NCP density only slightly lower than that displayed by X-ray; the two-start most compact structures can be unfolded with no DNA−DNA overlaps during the unfolding pathway.

The model, at this stage, is still homogeneous (i.e. the parameters are the same for each NCP): the heterogeneity of the NCP chain can be easily included in the Monte Carlo scheme, both at fixed and at variable temperatures (generalized ensemble Monte Carlo). However, the model shows that the two-start organization is not more intricate than the one-start organization. It is rather simple and can be obtained by a progressive side-by-side coiling of two columns, these latter strongly favored by anisotropic interactions. An almost straight linker connects the two helices. The most compact structures that more resemble the structure proposed on the basis of the X-ray data of the tetranucleosome can be easily unfolded without creating DNA entanglements.

Acknowledgment. This work has been done with the financial support of the FIRB 2001 project RBA01Y3SN of MIUR (Italy). The authors acknowledge Prof. Eligio Patrone (Cnr-ISMac) for stimulating discussions.

References and Notes

(1) Widom, J. *Annu. Rev. Biophys. Biomol. Struct.* **1998**, *27*, 285−327.
(2) Zlatanova, J.; Leuba, S. H. K. *Biophys. J.* **1998**, *74*, 2554−2566.
(3) Schiessel, H. *J. Phys.-Cond. Mat.* **2003**, *15*, R699−R774.
(4) Luger, K.; Mäder, A. W.; Richmond, R. K.; Sargent, D. F.; Richmond, T. J. *Nature (London)* **1997**, *389*, 251−260.
(5) Davey, C. A.; Sargent, D. F.; Luger, K.; Maeder, A. W.; Richmond, T. J. *J. Mol. Biol.* **2002**, *319*, 1097−1113.
(6) Widom, J. *Proc. Natl. Acad. Sci. U.S.A.* **1992**, *89*, 1095−1099.
(7) Woodcock, C. L.; Grigoryev, S. A.; Horowitz, R. A.; Whitaker, N. *Proc. Natl. Acad. Sci. U.S.A.* **1993**, *90*, 9021−9025.

(8) Robinson, P. J. J.; Rhodes, D. *Curr. Opin. Struct. Biol.* **2006**, *16*, 336−343.
(9) Finch, J. T.; Klug, A. K. *Proc. Natl. Acad. Sci. U.S.A.* **1976**, *73*, 1897−1901.
(10) Woodcock, C. L. F.; Frado,. Y.; Rattner, J. B. *J. Cell Biol.* **1984**, *99*, 42−52.
(11) Williams, S. P.; Athey, B. D.; Muglia, L. J.; Scott Schappe, R.; Gough, A. H.; Langmore, J. P. *Biophys. J.* **1986**, *49*, 233−248.
(12) Dorigo, B.; Schalch, T.; Kulangara, A.; Duda, S.; Schroeder, R. R.; Richmond, T. J. *Science* **2004**, *306*, 1571−1573.
(13) Schalch, T.; Duda, S.; Sargent, D. F.; Richmond, T. J. *Nature (London)* **2005**, *436*, 138−141.
(14) Lesne, A.; Victor, J.-M. *Eur. Phys. J. E* **2006**, *19*, 279−290.
(15) Shi, Y.; Hearst, J. E. *J. Chem. Phys.* **1994**, *101*, 5186−5200.
(16) Shi, Y.; Borovik, A. E.; Hearst, J. E. *J. Chem. Phys.* **1995**, *103*, 3166−3183.
(17) Leuba, S. H.; Yang, G.; Roberti, C.; Samori, B.; Zlatanova, K. J.; Bustamante, C. *Proc. Natl. Acad. Sci. U.S.A.* **1994**, *91*, 11621−11625.
(18) Bishop, T. C.; Hearst, J. E. *J. Chem. Phys.* **1998**, *102*, 6433−6439.
(19) Schiessel, H.; Gelbart, W. M.; Bruinsma, R. *Biophys. J.* **2001**, *80*, 1940−1956.
(20) Ben-Haïm, E.; Lesne, A.; Victor, J.-M. *Phys. Rev. E* **2001**, *64*, 05**1921**,1−19.
(21) Beard, D. A.; Schlick, T. *Structure* **2001**, *9*, 105−114.
(22) Wedemann, G.; Langowski, J. *Biophys. J.* **2002**, *82*, 2847-2859.
(23) Besker, N.; Anselmi, C.; Paparcone, R.; Scipioni, A.; Savino, M. P. *FEBS Lett.* **2003**, *554*, 369−372.
(24) Besker, N.; Anselmi, C.; P. *Biophys. Chem.* **2005**, *115*, 139−143.
(25) Leforestier, A.; Fudaley, S.; Livolant, F. *J. Mol. Biol.* **1999**, *290*, 481−494.
(26) Mangenot, S.; Leforestier, A.; Durand, D.; Livolant, F. *J. Mol. Biol.* **2003**, *333*, 907−916.
(27) Livolant, F.; Mangenot, S.; LeForestier, A.; De Frutos, A. B. M.; Raspaud, E.; Durand, D. *Philos. Trans. R. Soc. A* **2006**, *364*, 2615−2633.
(28) Lorman, V.; Podgornik, R.; Zeks, B. *Europhys. Lett.* **2005**, *69*, 1017−1023.
(29) Mangenot, S.; Raspaud, E.; Tribet, C.; Belloni, L.; Livolant, F. *Eur. Phys. J. E* **2002**, *7*, 221−231.
(30) Manning, G. S. *J. Am. Chem. Soc.* **2003**, *125*, 15087−15092.
(31) Perico, A.; La Penna, G.; Arcesi, L. *Biopolymers* **2006**, *81*, 20−28.
(32) Arcesi, L.; La Penna, G.; Perico, A. *Biopolymers* **2007**, *86*, 127−135.
(33) Le Penna, G.; Furlan, S.; Perico, A. *Biopolymers* **2006**, *83*, 135−147.
(34) Podgornik, R. *J. Chem. Phys.* **2003**, *118*, 11286−11296.
(35) Mühlbacher, F.; Holm, C.; Schiessel, H. *Europhys. Lett.* **2006**, *73*, 135−141.
(36) Hansen, J. P.; Donald, I. R. M. *Theory of Simple Liquids*; Academic Press: London 2006.
(37) Gay, J. G.; Berne, B. J. *J. Chem. Phys.* **1981**, *74*, 3316−3319.
(38) Bates, M. A.; Luckhurst, G. R. *Struct. Bonding (Berlin)* **1999**, *94*, 65−137.
(39) Zannoni, C. *J. Mater. Chem.* **2001**, *11*, 2637−2646.
(40) Zewdie, H. *Phys. Rev. E* **1998**, *57*, 1793−1805.
(41) Cinacchi, G.; Tani, A. *J. Chem. Phys.* **2002**, *117*, 11388−11395.
(42) Stone, A. J. *Mol. Phys.* **1978**, *36*, 241−256.
(43) Veerman, J. A. C.; Frenkel, D. *Phys. Rev. A* **1992**, *45*, 5632−5648.
(44) De Luca, M. D.; Neal, M. P.; Care, C. M. *Liq. Cryst.* **1994**, *16*, 257−266.
(45) Cui, Y.; Bustamante, C. *Proc. Natl. Acad. Sci. U.S.A.* **2000**, *97*, 127−132.
(46) La Penna, G. *J. Chem. Phys.* **2003**, *119*, 8162−8174.
(47) La Penna, G.; Morante, S.; Perico, A.; Rossi, G. C. *J. Chem. Phys.* **2004**, *121*, 10725−10741.
(48) Travers, A. *DNA−protein interactions*; Chapman & Hall: London, 1994, Chapter 3, p 14.
(49) Eisenhaber, F.; Lijnzaad, P.; Argos, P.; Sander, C.; Scharf, M. *J. Comput. Chem.* **1995**, *16*, 273−284.
(50) Li, W.; Dou, S.-X.; Wang, P.-Y. *J. Theor. Biol.* **2005**, *235*, 365−372.
(51) Bartolomé, S.; Bermúdez, A.; Daban, J.-R. *J. Cell Sci.* **1994**, *107*, 2983−2992.
(52) Livolant, F.; Leforestier, A. *Biophys. J.* **2000**, *78*, 2716−2729.
(53) Zlatanova, J.; Leuba, S. H.; K. *Crit. Rev. Eukaryot. Gene Expr.* **1999**, *9*, 245−250.
(54) Arsuaga, J.; Vazquez, M.; Trigueros, P. M. S.; Sumners, D.; Roca, J. *Proc. Natl. Acad. Sci. U.S.A.* **2005**, *102*, 9165−9169.
(55) Robinson, P. J. J.; Fairall, L.; Huynh, V. A. T.; Rhodes, D. *Proc. Natl. Acad. Sci. U.S.A.* **2006**, *103*, 6506−6511.
(56) Humphrey, W.; Dalke, A.; Schulten, K. *J. Mol. Graphics* **1996**, 14, 33−38. http://www.vmd.org.

MA071343L